Nano Energy 76 (2020) 105026

Contents lists available at ScienceDirect

Nano Energy

journal homepage: http://www.elsevier.com/locate/nanoen

Sub-nanometer-scale fine regulation of interlayer distance in Ni–Co layered double hydroxides leading to high-rate supercapacitors

Jie Zhao, Chengxuan Ge, Zhiyang Zhao, Qiang Wu **, Meng Liu, Minglei Yan, Lijun Yang, Xizhang Wang, Zheng Hu *

Key Laboratory of Mesoscopic Chemistry of MOE, School of Chemistry and Chemical Engineering, Nanjing University, Nanjing, 210023, China

ARTICLE INFO

Keywords:
Layered double hydroxides
Intercalation
Sub-nanometer-scale fine regulation
Supercapacitors
High-rate capability

ABSTRACT

Ni–Co layered double hydroxides (LDHs) have high theoretical capacities for energy storage by ion intercalation/release but suffer from the sluggish charge transport kinetics, hence are unsuitable for high-power supercapacitors nowadays. Herein, by intercalating the guest multi-carboxylic anions with straight-chain or conjugated-plane configurations, we have realized the sub-nanometer-scale fine regulation of the interlayer distance in Ni–Co LDHs for tuning the charge (ions and electrons) transport kinetics. With increasing the interlayer distance, the equivalent series resistance (R_{ESR}) shows the "inverted-volcano" evolution, which is first demonstrated for the anion-intercalated LDHs. With the smallest R_{ESR}, the LDH pillared by the conjugated 1,4-benzenedicarboxylic anion achieves the best matching between ion diffusion and electron transfer, and thus presents a high capacitance of 2115 F g^{-1} at 1 A g^{-1} and a record-high rate capability for the powder-like LDHs with the capacitance of 410 F g^{-1} at an ultrahigh current density of 150 A g^{-1}. The corresponding hybrid supercapacitor coupled with activated carbon presents the high energy density of 11.2 Wh kg^{-1} at the ultrahigh power density of 30.7 kW kg^{-1}, ranking at the top level for the supercapacitors based on the powder-like LDHs active materials. The minimal R_{ESR} from the "inverted-volcano" evolution could provide a feasible criterion to explore the high-rate LDH electrodes.

1. Introduction

Supercapacitors feature high power density and long cycle life, showing wide applications in electric devices needing high-power output [1–3]. Currently, great effort has been devoted to improving the energy density without scarifying the rate capability [4–6]. In this regard, developing advanced electrode materials based on faradaic redox reactions is highly attractive owing to their high theoretical capacities [7,8]. However, the redox-based electrode materials usually show a poor rate performance owing to the slow kinetics of charge (ions and electrons) transport [9–11]. The current innovations on redox materials are mainly limited to the achievement of high energy density at relatively low current density [12–15]. But the charge/discharge capability at high current density is actually essential to the supercapacitor applications, which is a highly challenging topic for redox materials.

Layered double hydroxides (LDHs), which are composed of positively charged brucite-like host layers of metal cations coordinated to hydroxide anions with some intercalated guest anions/molecules, have exhibited great promise in advanced electrochemical energy storage (EES) in virtue of their high theoretical capacities, low cost and controllable synthesis. The general formula of LDHs is $[M^{2+}_{1-x}M^{3+}_{x}(OH)_2]^{x+}$ $[A^{n-}_{x/n}]^{x-}\cdot mH_2O$, where M^{2+} and M^{3+} represent the bivalent and trivalent metal cations, respectively; A^{n-}, the charge-balancing anions; x, the surface charge determined by the ratio of two metal cations, i.e. $x = M^{3+}/(M^{2+}+M^{3+})$ [16,17]. The interlayer distance of LDHs intercalated by the typical CO_3^{2-} anions is about 0.77 nm [18]. During charge/discharge of LDHs, the reversible conversion between hydroxides and oxyhydroxides occurs in association with the shuttling of OH^- ions between the brucite-like layers [19]. In principle, the specific capacity is determined by the participation degree of LDHs in the redox reaction, and the rate capability is correlated with the transport kinetics of OH^- ions and electrons [20]. For the widely studied Ni (or Co)-based LDHs, the slow solid-state diffusion of OH^- ions between the brucite-like layers would limit the redox reaction kinetics and the

* Corresponding author.
** Corresponding author.
E-mail addresses: wqchem@nju.edu.cn (Q. Wu), zhenghu@nju.edu.cn (Z. Hu).

https://doi.org/10.1016/j.nanoen.2020.105026
Received 9 January 2020; Received in revised form 5 May 2020; Accepted 28 May 2020
Available online 20 June 2020

participation degree of active components, leading to the inferior EES performances especially at high current density. Many efforts have been devoted to improving the transport kinetics of OH^- ions or electrons, e.g., by designing nanoscale architectures [21], hybridizing with carbon materials [22–24], depositing on conductive substrates [19] or doping with other metals [25], which however shows the limited enhancement to the rate capability. To date, the high-threshold current density for Ni (or Co)-based LDHs is usually below 50 A g^{-1}, especially for the powder-like LDH active materials which have the advantages suitable for mass production and loading on different current collectors with tunable amount [26]. Such a poor rate capability cannot meet the requirement of supercapacitors aiming for the high-rate performance.

An intuitive solution is to enlarge the interlayer distance of LDHs, which could facilitate the solid-state diffusion of OH^- ions between the brucite-like layers, thus enhance the rate capability. By exchanging the charge-balancing anions (usually CO_3^{2-}, NO_3^-) using the long-chain ones with single negatively-charged end such as dodecyl sulfate (DS^-) [27–29] and dodecylbenzene sulfonate (DBS^-) [30], the interlayer distance has been roughly enlarged (Table S1). But the correlation of rate performance with interlayer distance is unclear to date, and the obtained rate performance is still below 50 A g^{-1} [27–30]. In this study, by pillaring the brucite-like layers using the long-chain anions with multiple negatively-charged ends, i.e., the multi-carboxylic anions of straight-chain or conjugated-plane configurations, we have realized the sub-nanometer-scale fine regulation of the interlayer distance in Ni–Co LDHs to tune the charge (ions and electrons) transport kinetics. With increasing the interlayer distance, the equivalent series resistance (R_{ESR}) shows the "inverted-volcano" evolution, which is first demonstrated for the anion-intercalated LDHs. With the smallest R_{ESR}, i.e., with the best matching between ion diffusion and electron transfer, the intercalated LDH sample by 1,4-benzenedicarboxylic presents a high capacitance of 2115 F g^{-1} at 1 A g^{-1}, and a record-high rate capability for the powder-like LDHs with the capacitance of 410 F g^{-1} at an ultrahigh current density of 150 A g^{-1}. The minimal R_{ESR} from the "inverted-volcano" evolution could provide a feasible criterion to explore the high-rate LDHs.

2. Experimental section

2.1. Synthesis of the pristine Ni–Co LDH

$Ni(NO_3)_2{\cdot}6H_2O$ (17.5 mmol, 5.089 g) and $Co(NO_3)_2{\cdot}6H_2O$ (2.5 mmol, 0.728 g) were dissolved in 100 mL distilled water and stirred for 30 min at room temperature. Then, 10 mL of degassed aqueous solution containing hexamethylenetetramine (HMT, 20 mmol, 2.804 g) and $H_2C_2O_4{\cdot}2H_2O$ (0.10 g) was added dropwise by a syringe below 40 °C under stirring. The transparent green solution was refluxed at 100 °C for 6 h under the protection of oxygen atmosphere to avoid CO_2 interference and favor the formation of Co^{3+}. After filtrating, repeated washing with deionized water and ethanol, and drying in vacuum oven at 80 °C, the pristine Ni–Co LDH was obtained with the intercalated NO_3^- ions, denoted as LDH/NO_3^-.

2.2. Synthesis of the Ni–Co LDHs intercalated/adsorbed by CO_3^{2-} or various carboxylic ions

For CO_3^{2-} intercalation, the pristine LDH/NO_3^- (0.100 g) and Na_2CO_3 (10 mmol, 1.060 g) were added into 100 mL degassed distilled water and refluxed at 90 °C for 24 h under oxygen atmosphere. Then, the product was obtained by filtrating, washing and drying, denoted as LDH/CO_3^{2-}. Similarly, for the straight-chain dicarboxylic anions intercalation, Na_2CO_3 was replaced with disodium succinate ($C_2H_4(COO)_2Na_2$), disodium adipate ($C_4H_8(COO)_2Na_2$) and disodium sebacate ($C_8H_{16}(COO)_2Na_2$), and the products were denoted as LDH/S4, LDH/S6, and LDH/S10, respectively. For the conjugated-plane multi-carboxylic anions intercalation, Na_2CO_3 was replaced with 1,3,5-benzenetricarboxylic sodium ($C_6H_3(COO)_3Na_3$), 2,6-naphthalenedicarboxylic sodium ($C_{10}H_6(COO)_2Na_2$), 1,4-benzenedicarboxylic sodium ($C_6H_4(COO)_2Na_2$) and perylene-3,4,9,10-tetracarboxylic sodium ($C_{20}H_8(COO)_4Na_4$), and the products were denoted as LDH/CBT, LDH/CND, LDH/CBD and LDH/CPT, respectively. For comparison, the LDHs adsorbed by the corresponding guest anions were obtained similarly by mixing the reactants at room temperature for 10 min, then filtrating and drying, i.e., without the process for refluxing at 90 °C for 24 h and washing (Fig. S1).

2.3. Materials characterization

The morphology and structure of the samples were characterized by scanning electron microscopy (SEM, Hitachi S-4800), transmission electron microscopy (TEM, JEM-2100F) and X-ray diffraction (XRD, Bruker D8 Advance A25 Co K_α radiation of 1.7902 Å). Fourier transform infrared spectroscopy (FT-IR, Bruker VERTEX70) was used to examine the anion species in LDHs. X-ray photoelectron spectroscopy (XPS, VG ESCALAB MKII) was used to analyze the composition of products. Inductively coupled plasma-mass spectrum (ICP-MS) was examined on an Optima 5300DV mass spectrometer. N_2 adsorption-desorption isotherms of the powder samples were measured at 77 K (Thermo Fisher). The specific surface area was obtained by the BET (Brunauer-Emmett-Teller) method and the pore size distribution was calculated from the adsorption branch of N_2 isotherms by the Barrett-Joyner-Halenda method. Atomic force microscopy (AFM, CSPM5500) was employed to measure the thickness of LDH nanosheet. The electrical conductivity of the pressed samples was measured by a four-probe method using a source measure unit (Keithley 6430).

2.4. Preparation of the working electrode

The working electrode was prepared by the drop-coating technique suitable for mass production on different current collectors with tunable loadings. Specifically, a slurry was firstly prepared by mixing LDH powders, acetylene black and poly(vinylidene fluoride) with a mass ratio of 8:1.5:0.5 in N-methyl-2-pyrrolidone. The slurry was dropped on a Ni foam (diameter 1.4 cm), then dried in vacuum at 80 °C for 12 h and pressed at 5 MPa. The obtained working electrode has the LDHs loading of ~1.5 mg (i.e., ~1.0 mg cm^{-2}), except for two control electrodes for LDH/CBD with the loading of 6.2 and 9.7 mg cm^{-2}.

2.5. Electrochemical measurements

The electrochemical performances of the electrodes were evaluated on a VMP3 workstation (Biologic) by using a three-electrode cell in 6 M KOH electrolyte, with platinum foil counter electrode and Ag/AgCl reference electrode (with a salt bridge of 3 M KCl aqueous solution). The specific capacitance (C_s, F g^{-1}) was calculated by the following equation: $C_s = (I \times \Delta t)/(m \times \Delta V)$, where I is the discharge current (A), Δt is the discharge time (s), ΔV is the potential range (V), and m is the mass of the used LDH (g). For comparision, the electrochemical performance contributions of the bare Ni foams were also measured and calculated.

2.6. Fabrication and evaluation of hybrid supercapacitors

The hybrid supercapacitor was assembled with LDH/CBD (the positive material), AC (the negative material), 6 M KOH (the electrolyte), and a cellulose acetate membrane (the separator), denoted as LDH/CBD//AC. The mass loading ratio of LDH/CBD to AC is matched to be 1 : 3.7. The energy density (E) and power density (P) of the device was calculated by the following integral formulas:

$$E = (I / M) \int V(t)\, dt$$

$$P = E / \Delta t$$

Here, I is the discharge current (A), M is the total mass of the positive and negative materials (g), $\int V(t)\,dt$ is the area under the galvanostatic discharge curve (V·s), Δt is the discharge time (s). The LDH/NO_3^-//AC, LDH/CO_3^{2-}//AC hybrid supercapacitor and AC//AC symmetric supercapacitor were also fabricated via the same procedure for comparison.

3. Results and discussion

3.1. Sub-nanometer-scale fine regulation of the interlayer distance

The pristine Ni–Co LDH sample was obtained by refluxing the aqueous solution of $Ni(NO_3)_2$, $Co(NO_3)_2$ and hexamethylenetetramine (HMT) at 100 °C for 6 h, similar to our recent study [31]. The as-prepared Ni–Co LDH intercalated by NO_3^- ions was denoted as LDH/NO_3^-, which presents the hierarchical spherical morphology assembled by the thin nanosheets with thickness of several nanometers and interlayer distance of 0.823 nm (Fig. S2). Fig. 1 shows the replacement of NO_3^- with CO_3^{2-} or various multi-carboxylic anions. Different from the case of DS^- or DBS^- ions with only one negatively-charged end, the multi-carboxylic anions could bind with the neighboring positively-charged brucite-like layers by electrostatic interaction and hydrogen bonds (Fig. 1a), which leads to a sub-nanometer-scale fine regulation of the interlayer distances while remaining the hierarchical spherical morphologies (Figs. S1 and S3 and Table S1). Specifically, by replacing NO_3^- with CO_3^{2-} anions, the XRD characteristic (003) peak shifts from 2θ of 12.49° to the higher angle of 13.44° owing to the narrowing of the interlayer distance from 0.823 to 0.765 nm. On the contrary, with the multi-carboxylic anions, the characteristic peak generally shifts to the lower angle side due to the wider interlayer distances (Fig. 1b). For the straight-chain dicarboxylic anions, the interlayer distances are increased to 0.881, 0.945 and ~1.247 nm for LDH/S4, LDH/S6 and LDH/S10, respectively. For the conjugated-plane multi-carboxylic anions, the interlayer distances are tuned to 0.820, 0.842, 0.908 and 0.932 nm for LDH/CBT, LDH/CND, LDH/CBD and LDH/CPT, respectively. The interlayer distance of LDHs versus the anion length shows a quasi-linear relationship, indicating the fine regulation of interlayer distances by tuning the anion length (Fig. 1c and Fig. S4). The widened interlayer distance favors the shuttling of OH^- ions between the brucite-like layers during charging/discharging to achieve the high-rate capability.

3.2. Structure characterization

The typical LDH/CBD sample was well characterized by SEM and TEM, as shown in Fig. 2. The sample presents a porous spherical architecture with the size of 3–8 μm, which is assembled by the radial-aligned thin nanosheets with a submicrometer interspace (Fig. 2a and b). The nanosheets are highly wrinkled and intercrossed with the average thickness of 6–8 nm, i.e., about 7–9 brucite-like layers (Fig. S5). TEM images indicate that the LDH/CBD possesses numerous holes in the wrinkled nanosheets (Fig. 2c and d). High-resolution TEM (HRTEM) image shows the (003) fringes with a large interlayer distance of 0.91 nm (Fig. 2e), in agreement with the XRD characterization (Fig. 1b). Such a unique architecture leads to a high specific surface area of 135.3 $m^2 g^{-1}$ and a coexisting meso-, and macropores, favorable for electrolyte access during EES (Fig. S6). The representative TEM image and corresponding elemental mappings indicate the uniform distribution of Ni, Co, O and C elements (Fig. 2f–j). XPS and ICP-MS give the Ni/Co atomic ratio of ca. 13.3 (Fig. S7 and Table S2).

3.3. Charge transport kinetics

The preceding results indicate that we have obtained the series of hierarchical Ni–Co LDHs with the widened interlayer distance which

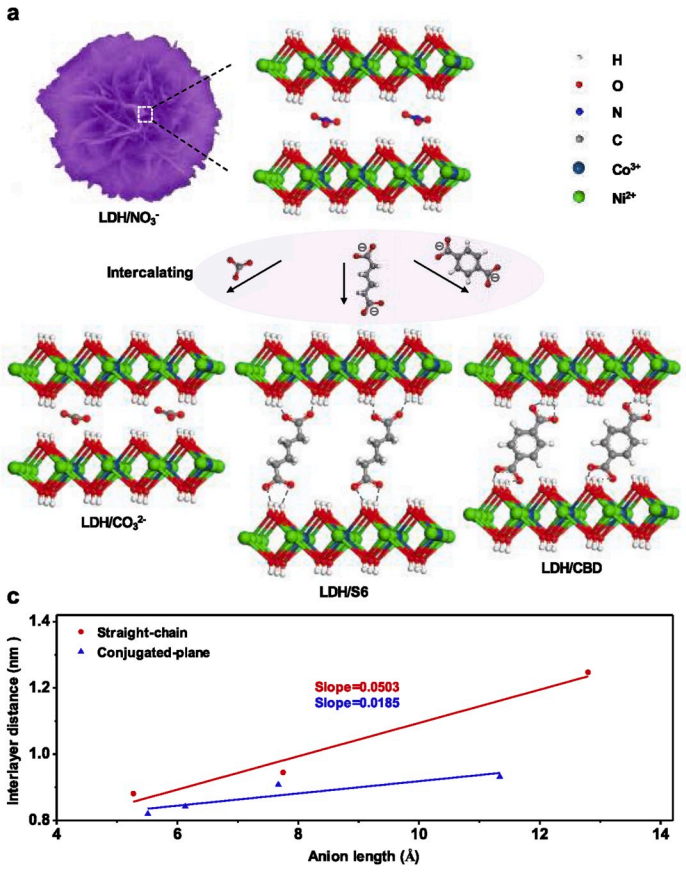

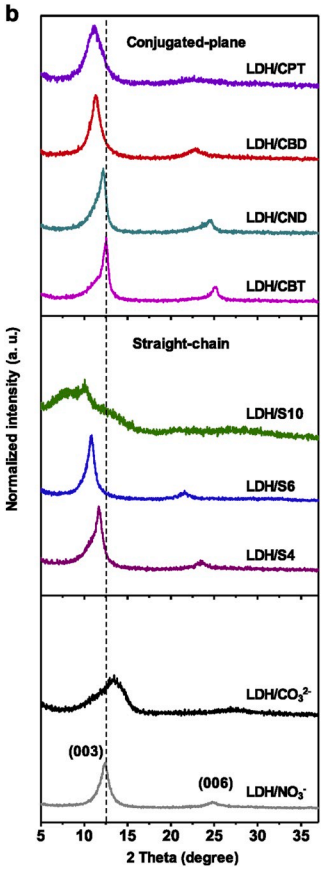

Fig. 1. Sub-nanometer-scale regulation of the interlayer distance in Ni–Co LDHs by anion intercalation. (a) Schematic illustration for the anion intercalation of the Ni–Co LDHs. (b) XRD patterns of the Ni–Co LDHs with different intercalated anions. (c) Interlayer distance versus length of the intercalated anions. Note: S4_$[C_2H_4(COO)_2]^{2-}$, S6_$[C_4H_8(COO)_2]^{2-}$, S10_$[C_8H_{16}(COO)_2]^{2-}$, CBT_$[C_6H_3(COO)_3]^{3-}$, CND_$[C_{10}H_6(COO)_2]^{2-}$, CBD_$[C_6H_4(COO)_2]^{2-}$, CPT_$[C_{20}H_8(COO)_4]^{4-}$. The formulas of these anions are shown in Fig. S4.

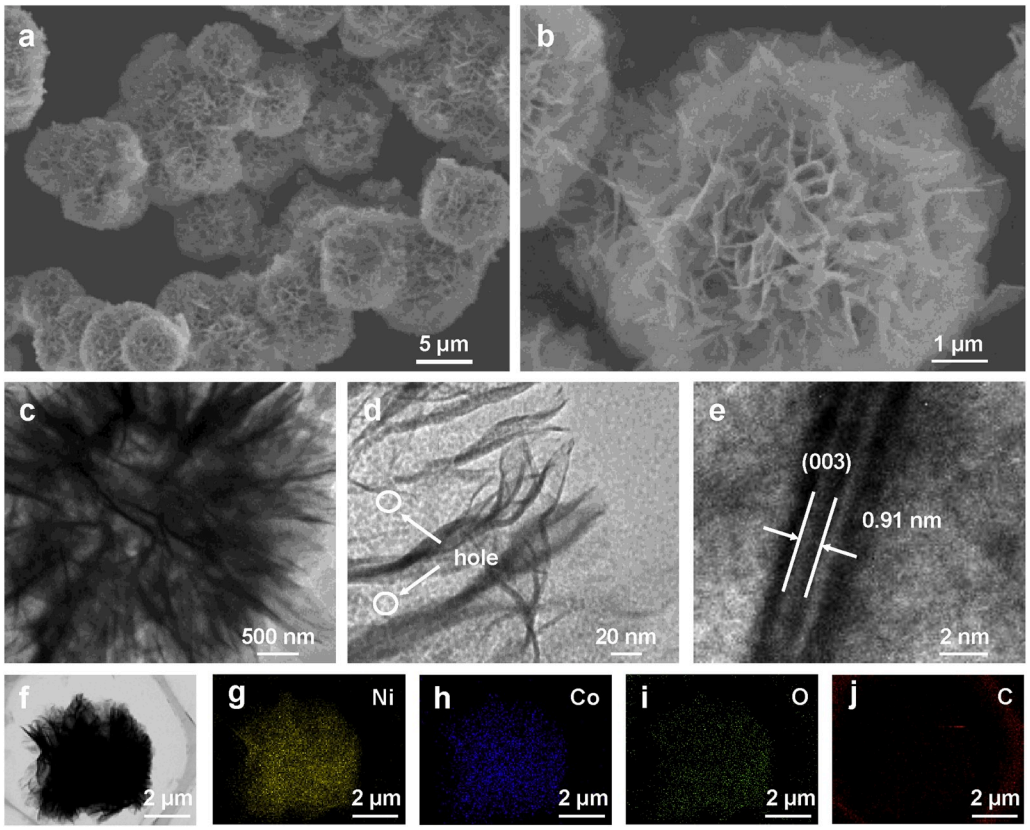

Fig. 2. Microstructure of a typical LDH/CBD sample. (a, b) SEM images. (c, d) TEM images. (e) HRTEM image, showing (003) fringe with a spacing of 0.91 nm. (f–j) TEM image and the corresponding elemental mappings of Ni, Co, O and C. Note: The C signal came from the intercalated anions with high uniformity.

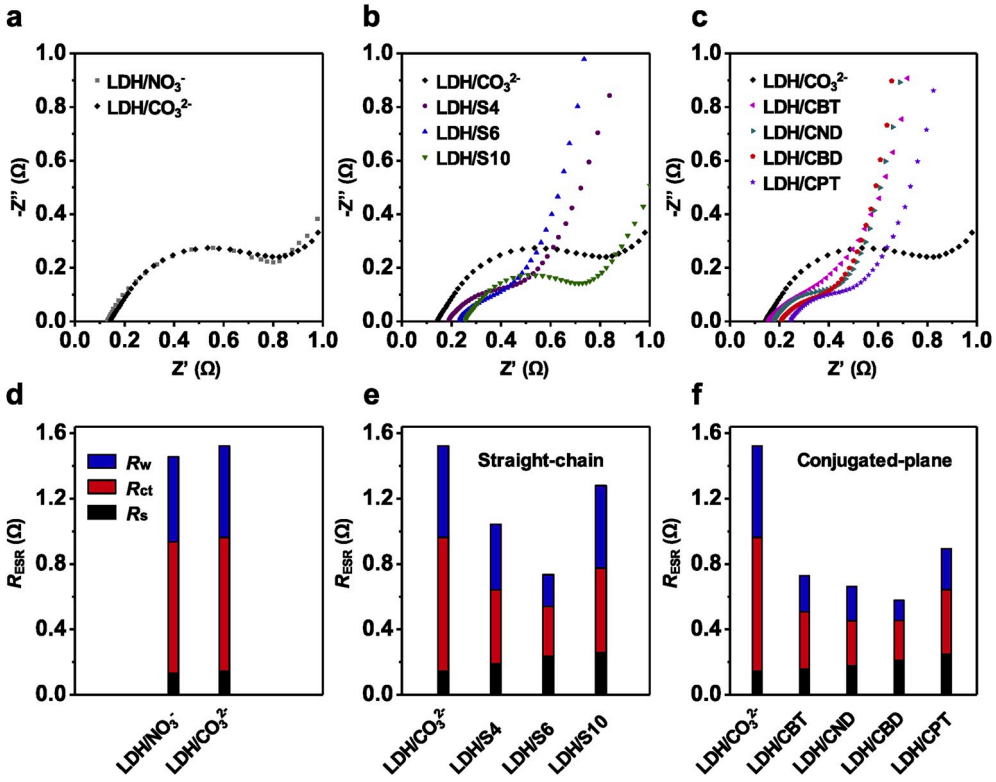

Fig. 3. Electrochemical impedance spectra characterization. (a–c) Nyquist plots at high frequency. (d–f) The intrinsic Ohmic resistance (R_s), charge transfer resistance (R_{ct}), Warburg resistance (R_w) and equivalent series resistance (R_{ESR}). Note: $R_{ESR} = R_s + R_{ct} + R_w$.

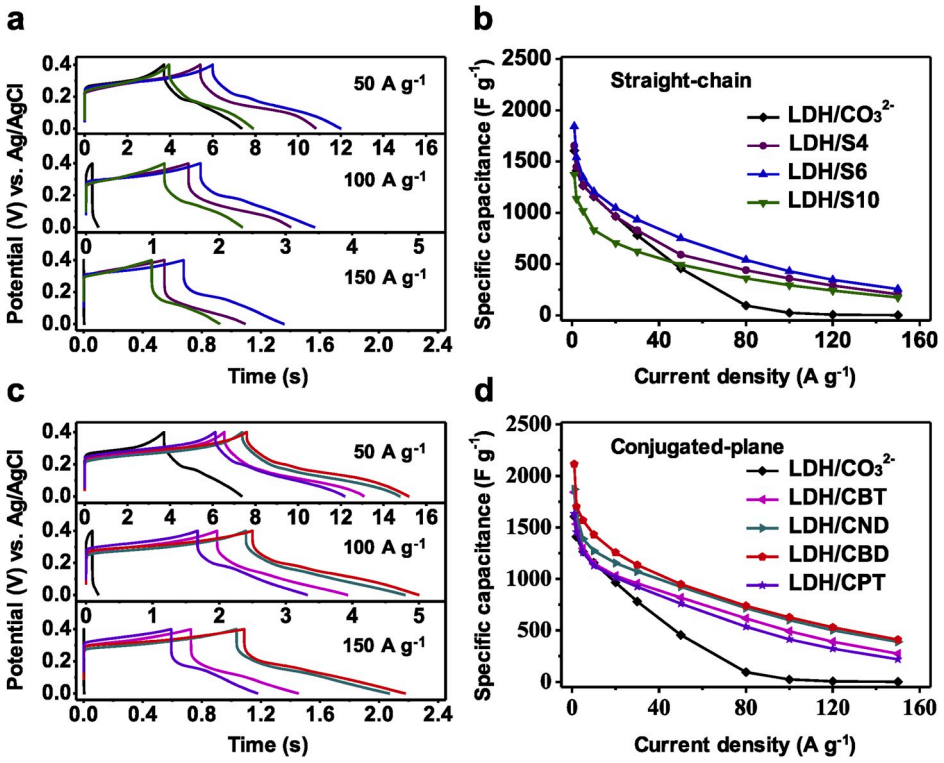

Fig. 4. Electrochemical performances of the straight-chain and the conjugated-plane configuration system. (a, c) Galvanostatic charge/discharge curves at 50, 100 and 150 A g^{-1}. (b, d) Specific capacitances at 1–150 A g^{-1}. Note: The areal loading is 1.0 mg cm^{-2}.

should be favorable for the solid-state diffusion of OH^- ions between the brucite-like layers. The influence of interlayer distance on the charge (ions and electrons) transport kinetics was characterized by the electrochemical impedance spectra (EIS), as shown in Fig. 3. The LDH/CO_3^{2-} presents the similar Nyquist plot to the pristine LDH/NO_3^-, with the close intrinsic Ohmic resistance (R_s), and the slightly larger charge transfer resistance (R_{ct}) and Warburg resistance (R_w) for the former due to the decreased interlayer distance (Fig. 3a,d and Table S3). R_{ct} mainly comes from the electronic and ionic resistances at the interface between the electrode and the electrolyte, and R_w is closely related to the resistance for OH^- diffusion from electrolyte into the brucite-like layers in this case (Fig. S8). Due to the equilateral triangle structure, CO_3^{2-} ion can be regarded either as the straight-chain or as the conjugated-plane anion. For the LDHs intercalated by either the straight-chain or the conjugated-plane anions, R_s presents a rational increase with increasing the interlayer distance. The former is in the order of LDH/CO_3^{2-} < LDH/S4 < LDH/S6 < LDH/S10 (Fig. 3b and e), and the latter is in the order of LDH/CO_3^{2-} < LDH/CBT < LDH/CND < LDH/CBD < LDH/CPT (Fig. 3c and f), respectively, in consistence with the changes of the corresponding bulk conductivities (Fig. S9). In contrast, R_{ct} and R_w present a tendency of first decrease then increase with increasing the interlayer distance. Accordingly, the equivalent series resistance ($R_{ESR} = R_s + R_{ct} + R_w$) presents an "inverted-volcano" evolution, i.e., first decrease then increase (Fig. 3e and f).

This "inverted-volcano" evolution is somewhat different from our initial intuition, but could be understood by analyzing the influence of interlayer distance on the charge (ions and electrons) transport kinetics. As known, the narrow interlayer distance favors the electron transfer but doesn't favor the OH^- diffusion between the brucite-like layers, leading to the corresponding small R_s and large R_{ct} and R_w (usually $R_s \ll R_{ct}$), and thus the high R_{ESR}. In this case, the rate-determining step is the OH^- diffusion for the redox reactions during charge/discharge of LDHs [32–34]. With widening the interlayer distance moderately, the R_s increases slowly, while R_{ct} and R_w decrease dramatically due to the much promoted OH^- diffusion, leading to the decreasing of R_{ESR} until the approach of R_s to R_{ct} and R_w (i.e., $R_s \approx R_{ct}$) with the minimal R_{ESR}. In this case, the rate-determining step is still the OH^- diffusion since enough electrons are available to match with the OH^- shuttling for the redox reactions. Further widening the interlayer distance leads to the continue increase of R_s. In this case, despite the favorable factor for the OH^- diffusion from geometrical viewpoint, the insufficient electrons to match with the OH^- for the redox reaction lead to an inverse increase of R_{ct} and R_w, and thus the quick increase of R_{ESR} (again $R_s \ll R_{ct}$) [35,36]. In other words, the rate-determining step shifts from the OH^- diffusion for the former two cases to the electron transfer for the last case (Fig. S10). Such an "inverted-volcano" evolution is well demonstrated either by the straight-chain (Fig. 3b and e) or by the conjugated-plane configuration system (Fig. 3c and f).

3.4. High-rate EES performances

Based on the preceding analysis, the best matching between ion diffusion and electron transfer should be obtained at the turning-point of the "inverted-volcano" evolution of R_{ESR}, which corresponds to the fastest diffusion of OH^- ions between the brucite-like layers, thus much enhances the rate capability (Fig. S11). Indeed, the sample with the smaller R_{ESR} presents the better rate capability either for the straight-chain or for the conjugated-plane configuration system, with the respective LDH/S6 and LDH/CBD the best due to the smallest R_{ESR}, as shown in Fig. 4 (Figs. S12 and S13 and Table S3). In other words, the

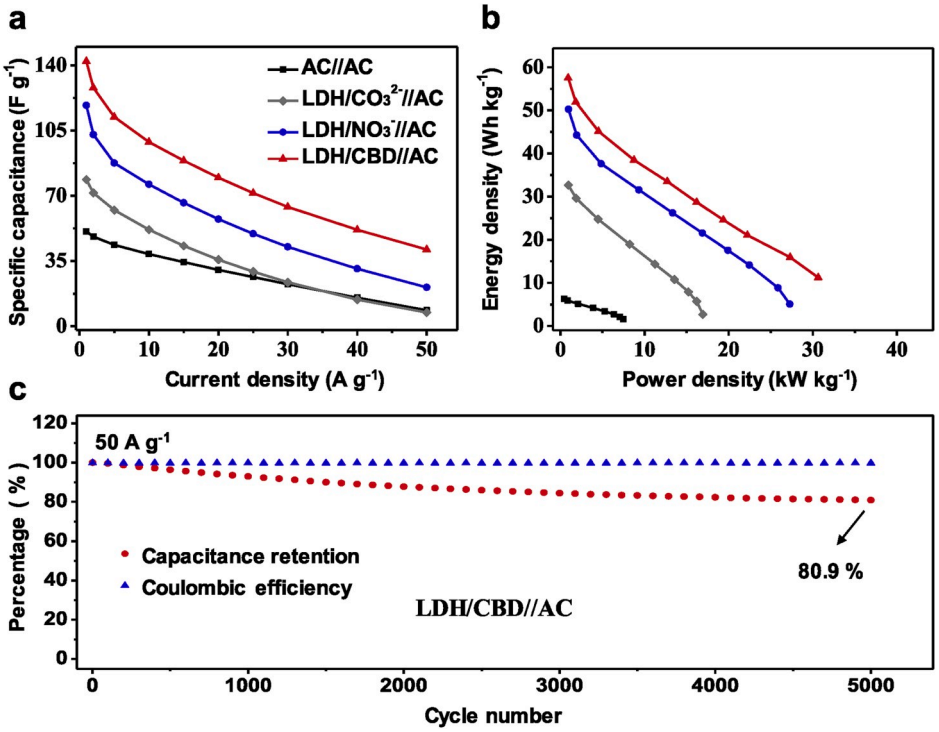

Fig. 5. Electrochemical performances of the supercapacitors. (a) Specific capacitances at 1–50 A g^{-1}. (b) Ragone plots. (c) Cycling performance of LDH/CBD//AC at 50 A g^{-1}.

minimal R_{ESR} from its "inverted-volcano" evolution can act as a criterion to screen the high-rate electrode materials. The LDH/S6 presents a high specific capacitance of 1844 F g^{-1} at 1 A g^{-1} and remains 255 F g^{-1} at the ultrahigh current density of 150 A g^{-1}. The LDH/CBD presents an even higher specific capacitance of 2115 F g^{-1} at 1 A g^{-1}, and a record-high rate capability for powder-like LDH with the capacitance of 410 F g^{-1} at the ultrahigh current density of 150 A g^{-1} (Figs. S14 and S15 and Table S4). The higher rate capability of LDH/CBD than LDH/S6 might be associated with the better electron mobility of the conjugated-plane CBD than the straight-chain S6 in the case of close interlayer distance [37–39]. In addition, the LDH/CBD also displays a rather good cycling stability of 76.7% capacitance retention after 5000 cycles at the ultra-high current density of 150 A g^{-1} with the Coulombic efficiency of ~100% (Fig. S16). When increasing the areal loading from 1.0 to 6.2 mg cm^{-2}, the LDH/CBD electrode still presents an excellent EES performance (from 410 to 222 F g^{-1} at 150 A g^{-1}), indicating the great potential for practical applications (Figs. S17 and S18).

3.5. Electrochemical evaluation of supercapacitors

The superior EES performance of LDH/CBD is also evaluated by the corresponding LDH/CBD//activated carbon (AC) hybrid supercapacitor, as shown in Fig. 5. The specific capacitance achieves as high as 142.2 F g^{-1} at 1 A g^{-1} and still retains 41.2 F g^{-1} even at a high current density of 50 A g^{-1}. In contrast, the hybrid supercapacitors of the LDH/NO_3^-//AC (118.6 and 20.8 F g^{-1}), LDH/CO_3^{2-}//AC (78.8 and 7.4 F g^{-1}), and the symmetric supercapacitor of AC//AC (50.8 and 8.6 F g^{-1}) present the obviously lower specific capacitances at corresponding current densities, respectively (Fig. 5a and Fig. S19). The LDH/CBD//AC displays a high energy density of 57.5 Wh kg^{-1} at a power density of 0.9 kW kg^{-1} (the discharge time of 227.7 s). Even at an ultrahigh power density of 30.7 kW kg^{-1} (the discharge time of 1.3 s), it still presents a top-level energy density of 11.2 Wh kg^{-1}, better than LDH/NO_3^-//AC (5.1 Wh kg^{-1} @ 27.3 kW kg^{-1}), LDH/CO_3^{2-}//AC (2.7 Wh kg^{-1} @ 16.9 kW kg^{-1}), and superior to most aqueous supercapacitors to date (Fig. 5b, Fig. S20 and Table S5). The LDH/CBD//AC also exhibits good cycling stability at a high current density of 50 A g^{-1}, which shows 80.9% capacitance retention after 5000 cycles with the Coulomb efficiency ~100% (Fig. 5c and Fig. S21). Two tandem LDH/CBD//AC can efficiently light two commercial LED indicators for 13 min, and one LDH/CBD//AC can power a timer over 22 h, demonstrating its great potential in applications (Video S1 and Fig. S22).

Supplementary video related to this article can be found at https://doi.org/10.1016/j.nanoen.2020.105026

4. Conclusion

In summary, by intercalating the guest multi-carboxylic anions with straight-chain or conjugated-plane configurations, we have realized the sub-nanometer-scale fine regulation of the interlayer distance in Ni–Co LDHs. With such a fine regulation, we first demonstrated the "inverted-volcano" evolution of the R_{ESR} with increasing the interlayer distance, which is well associated with the charge (ions and electrons) transport kinetics. The best matching between ion diffusion and electron transfer leads to the smallest R_{ESR} at the turning-point of its "inverted-volcano" evolution, which corresponds to the best supercapacitive performance. Accordingly, the LDH/S6 with the smallest R_{ESR} for the straight-chain configurations presents a high specific capacitance of 1844 F g^{-1} at 1 A g^{-1} and remains 255 F g^{-1} at the ultrahigh current density of 150 A g^{-1}. The LDH/CBD with the smallest R_{ESR} for the conjugated-plane

configurations presents an even higher specific capacitance of 2115 F g^{-1} at 1 A g^{-1}, and a record-high rate capability for the powder-like LDHs with the capacitance of 410 F g^{-1} at the ultrahigh current density of 150 A g^{-1}. Such performances overcome the limitation of the poor charge/discharge capability at high current density for the conventional LDH-based electrodes. The higher rate capability of LDH/CBD than LDH/S6 might be associated with the better electron mobility of the conjugated-plane CBD than the straight-chain S6 in the case of close interlayer distance. The superior EES performance of LDH/CBD is also well exhibited by the corresponding LDH/CBD//AC hybrid supercapacitor, which delivers an ultrahigh energy density of 11.2 Wh kg^{-1} at an ultrahigh power density of 30.7 kW kg^{-1} based on the powder-like LDH active materials. The minimal R_{ESR} from the "inverted-volcano" evolution could also provide a feasible criterion to explore the high-rate LDHs. Based on our understanding on the "inverted-volcano" evolution of R_{ESR}, the turning-point corresponding to the smallest R_{ESR} mainly results from the limited electron transfer with increasing the interlayer distance. It is speculated that further improving the electron transfer while increasing the interlayer distance should be a promising strategy to develop the high-rate electrode materials, e.g., by pillaring the brucite-like layers with conductive carbon layer or tiny metal nanoparticles or by growing the LDHs with large interlayer distance on the current collector. The intercalation strategy with multi-carboxylic anions can not only finely regulate the interlayer distance in sub-nanometer-scale but also be suitable for mass production, which is of great significance to develop the advanced LDHs-based supercapacitors for applications.

CRediT author statement

Z.H. and Q.W. conceived and supervised the project. J.Z. designed and performed the experiment. C.X.G., Z.Y.Z., M.L. and M.L.Y. helped with the measurements of TEM and SEM. Z.H., J.Z., Q.W., L.J.Y. and X.Z. W. evaluated the data and made the intensive discussion. J.Z., Q.W. and Z.H. wrote the manuscript. The manuscript was revised by all authors.

Declaration of competing interest

The authors declare no competing financial interest.

Acknowledgements

This work was jointly supported by the National Key Research and Development Program of China (2017YFA0206500, 2018YFA0209103), National Natural Science Foundation of China (21832003, 21773111, 51571110, 21573107, 21972061).

Appendix A. Supplementary data

Supplementary data to this article can be found online at https://doi.org/10.1016/j.nanoen.2020.105026.

References

[1] P. Simon, Y. Gogotsi, B. Dunn, Science 343 (2014) 1210–1211.
[2] C. Zhang, Nat. Energy 4 (2019) 170.
[3] K. Nomura, H. Nishihara, N. Kobayashi, T. Asada, T. Kyotani, Energy Environ. Sci. 12 (2019) 1542–1549.
[4] M.F. El-Kady, Y. Shao, R.B. Kaner, Nat. Rev. Mater. 1 (2016) 16033.
[5] M. Salanne, B. Rotenberg, K. Naoi, K. Kaneko, P.-L. Taberna, C.P. Grey, B. Dunn, P. Simon, Nat. Energy 1 (2016) 16070.
[6] Q. Wu, L. Yang, X. Wang, Z. Hu, Acc. Chem. Res. 50 (2017) 435–444.
[7] C. Tan, X. Cao, X.-J. Wu, Q. He, J. Yang, X. Zhang, J. Chen, W. Zhao, S. Han, G.-H. Nam, M. Sindoro, H. Zhang, Chem. Rev. 117 (2017) 6225–6331.
[8] A. Noori, M.F. El-Kady, M.S. Rahmanifar, R.B. Kaner, M.F. Mousavi, Chem. Soc. Rev. 48 (2019) 1272–1341.
[9] T. Ling, P. Da, X. Zheng, B. Ge, Z. Hu, M. Wu, X.-W. Du, W.-B. Hu, M. Jaroniec, S.-Z. Qiao, Sci. Adv. 4 (2018), eaau6261.
[10] H.-S. Kim, J.B. Cook, H. Lin, J.S. Ko, S.H. Tolbert, V. Ozolins, B. Dunn, Nat. Mater. 16 (2017) 454–460.
[11] B.-T. Liu, X.-M. Shi, X.-Y. Lang, L. Gu, Z. Wen, M. Zhao, Q. Jiang, Nat. Commun. 9 (2018) 1375.
[12] K.A. Owusu, L. Qu, J. Li, Z. Wang, K. Zhao, C. Yang, K.M. Hercule, C. Lin, C. Shi, Q. Wei, L. Zhou, L. Mai, Nat. Commun. 8 (2017) 14264.
[13] N. Feng, R. Meng, L. Zu, Y. Feng, C. Peng, J. Huang, G. Liu, B. Chen, J. Yang, Nat. Commun. 10 (2019) 1372.
[14] G. Yilmaz, K.M. Yam, C. Zhang, H. Fan, G.W. Ho, Adv. Mater. 29 (2017), 1606814.
[15] L. Shen, L. Yu, H.B. Wu, X.-Y. Yu, X. Zhang, X.W. Lou, Nat. Commun. 6 (2015) 6694.
[16] G. Fan, F. Li, D.G. Evans, X. Duan, Chem. Soc. Rev. 43 (2014) 7040–7066.
[17] J. Yu, Q. Wang, D. O'Hare, L. Sun, Chem. Soc. Rev. 46 (2017) 5950–5974.
[18] J. Zhao, J. Chen, S. Xu, M. Shao, Q. Zhang, F. Wei, J. Ma, M. Wei, D.G. Evans, X. Duan, Adv. Funct. Mater. 24 (2014) 2938–2946.
[19] G. Xiong, P. He, D. Wang, Q. Zhang, T. Chen, T.S. Fisher, Adv. Funct. Mater. 26 (2016) 5460–5470.
[20] X. Yu, S. Yun, J.S. Yeon, P. Bhattacharya, L. Wang, S.W. Lee, X. Hu, H.S. Park, Adv. Energy Mater. 8 (2018), 1702930.
[21] J. Yang, C. Yu, X. Fan, J. Qiu, Adv. Energy Mater. 4 (2014) 1400761.
[22] J. Chen, X. Wang, J. Wang, P.S. Lee, Adv. Energy Mater. 6 (2016), 1501745.
[23] X. Wu, L. Jiang, C. Long, T. Wei, Z. Fan, Adv. Funct. Mater. 25 (2015) 1648–1655.
[24] J. Yang, C. Yu, C. Hu, M. Wang, S. Li, H. Huang, K. Bustillo, X. Han, C. Zhao, W. Guo, Z. Zeng, H. Zheng, J. Qiu, Adv. Funct. Mater. 28 (2018), 1803272.
[25] M. Gong, Y. Li, H. Zhang, B. Zhang, W. Zhou, J. Feng, H. Wang, Y. Liang, Z. Fan, J. Liu, H. Dai, Energy Environ. Sci. 7 (2014) 2025–2032.
[26] M. Zhao, Q. Zhao, B. Li, H. Xue, H. Pang, C. Chen, Nanoscale 9 (2017) 15206–15225.
[27] Y. Xiao, D. Su, X. Wang, S. Wu, L. Zhou, S. Fang, F. Li, Sci. China Mater. 61 (2018) 263–272.
[28] L. Wang, Z.H. Dong, Z.G. Wang, F.X. Zhang, J. Jin, Adv. Funct. Mater. 23 (2013) 2758–2764.
[29] X. Liu, R. Ma, Y. Bando, T. Sasaki, Adv. Funct. Mater. 24 (2014) 4292–4302.
[30] Y. Lin, X. Xie, X. Wang, B. Zhang, C. Li, H. Wang, L. Wang, Electrochim. Acta 246 (2017) 406–414.
[31] H. Lai, Q. Wu, J. Zhao, L. Shang, H. Li, R. Che, Z. Lyu, J. Xiong, L. Yang, X. Wang, Z. Hu, Energy Environ. Sci. 9 (2016) 2053–2060.
[32] J. Chen, J. Xu, S. Zhou, N. Zhao, C.-P. Wong, Nano Energy 21 (2016) 145–153.
[33] Q. Wang, X. Wang, J. Xu, X. Ouyang, X. Hou, D. Chen, R. Wang, G. Shen, Nano Energy 8 (2014) 44–51.
[34] Z. Li, M. Shao, L. Zhou, R. Zhang, C. Zhang, J. Han, M. Wei, D.G. Evans, X. Duan, Nano Energy 20 (2016) 294–304.
[35] X. Wang, J. Zhang, S. Yang, H. Yan, X. Hong, W. Dong, Y. Liu, B. Zhang, Z. Wen, Electrochim. Acta 295 (2019) 1–6.
[36] L. Lv, K. Xu, C. Wang, H. Wan, Y. Ruan, J. Liu, R. Zou, L. Miao, K. Ostrikov, Y. Lan, J. Jiang, Electrochim. Acta 216 (2016) 35–43.
[37] L.O. Jones, M.A. Mosquera, G.C. Schatz, M.A. Ratner, J. Phys. Chem. B 123 (2019) 8096–8102.
[38] M.A. Reed, C. Zhou, C.J. Muller, T.P. Burgin, J.M. Tour, Science 278 (1997) 252–254.
[39] C. Yan, Z. Fang, C. Lv, X. Zhou, G. Chen, G. Yu, ACS Nano 12 (2018) 8670–8677.

Jie Zhao received his M.E. degree from Nanchang Hangkong University in 2015. He is currently a Ph.D. candidate under the supervision of Prof. Qiang Wu and Prof. Zheng Hu in School of Chemistry and Chemical Engineering, Nanjing University. His research interests mainly focus on the development of high-rate energy storage systems, addressing the charge/discharge mechanism and materials design.

Chengxuan Ge received her Bachelor's degree from Huazhong University of Science and Technology in 2017. She is currently a Master student under the supervision of Prof. Qiang Wu and Prof. Zheng Hu in School of Chemistry and Chemical Engineering, Nanjing University. Her research interests mainly focus on the NiCo-based materials for the aqueous supercapacitors.

Zhiyang Zhao is currently a M.S. candidate under the supervision of Prof. Lijun Yang and Prof. Zheng Hu in School of Chemistry and Chemical Engineering, Nanjing University. He received his B.S. degree from Nanjing University of Science and Technology in 2018. His research interests mainly focus on the theoretical understanding of the mechanisms in energy conversion and storage systems.

Qiang Wu obtained his Ph.D. from Nanjing University in 2004. He was appointed an associate professor in 2006, and a professor of Nanjing University in 2015. As a Hua-Ying Scholar, he visited Stanford University for one year. His scientific interests focus on the rational design of nano-/mesostructured materials and their applications in energy storage and conversion.

Meng Liu received her M.S. degree from Zhengzhou University of Light Industry in 2015 and obtained her Ph.D. from Nanjing University in 2020. Her research interests mainly focus on the development of new energy storage systems especially for Li-ion and Na-ion batteries, addressing the electrochemical mechanism and materials design.

Minglei Yan received his M.S. degree in School of Material Science and Engineering from Sichuan University in 2016. He is currently a Ph.D. candidate under the supervision of Prof. Zheng Hu in School of Chemistry and Chemical Engineering, Nanjing University. His research interests focus on the synthesis of transition metal-based materials with heterojunction and their application in energy conversion.

Lijun Yang received his Ph.D. in solid mechanics from Harbin Institute of Technology in 2006, and gradually converged to chemistry after two post-doc periods in IMEC Belgium and Nanjing University. Now he is an associate professor in Nanjing University and mainly focuses on the theoretical understanding of the mechanisms in energy conversion and storage systems, such as fuel cells, supercapacitors and lithium batteries.

Xizhang Wang received his Ph.D. in chemistry from Nanjing University in 2001. He was appointed an associate professor of Nanjing University in 2003 and full professor in 2011. He was a JSPS Fellow in Tokyo University (2003–2005). His scientific interests mainly focus on nanomaterial chemistry, sustainable energy, and heterogeneous catalysis.

Zheng Hu received his BS (1985) and Ph.D. (1991) degrees in physics from Nanjing University. After two-year's postdoctoral research in Department of Chemistry, he became an associate professor in 1993, and subsequently acquired the professor position in 1999, and Cheung Kong Scholar professor in 2007. He is the owner of the NSFC fund for outstanding young scientists of China (2005). Hu is engaged in the research field of physical chemistry and materials chemistry addressing the growth mechanism, materials design and energy applications of a range of nano-/mesostructured materials, especially the carbon-based materials, group III nitrides and transition metal oxides.